Global Vibration Control of Split Stirling Linear Cryogenic Cooler

A. Veprik[1], A. Tuito[2]

[1] SemiConductor Devices, POB 2250, Haifa, 31021, Israel
[2] Israel Ministry of Defense, Kirya, Tel Aviv, 64734, Israel

ABSTRACT

High operating temperature, low size, weight and power (SWAP) infrared imagers often rely on miniature split Stirling linear cryocoolers composed of an electro-dynamically driven compressor and a pneumatically driven expander. For compactness, the two compoents are mounted side-by-side to a common rigid frame and connected by a configurable transfer line.

Vibration export produced by such a cryocooler may be thought of as a pair of tonal and coherent forces resulting from the almost sinusoidal imbalanced reciprocation of the moving assemblies inside the compressor and expander. The cooler-induced vibration of the infrared imager is, therefore, comprised of a coupled angular and translational components manifesting themselves in the form of angular line of sight jitter and translational defocusing.

The authors present a Multimodal Tuned Dynamic Absorber, featuring translational and tilting dynamic modes, the frequencies which are essentially tuned to the fixed driving frequency. Dynamic analysis shows that the dynamic reactions (force and moment) produced by such a dynamic absorber may simultaneously attenuate both translational and angular components of cryocooler-induced vibration, and improve the quality of the imagery.

INTRODUCTION

Split Stirling linear micro-miniature cryocoolers find use in advanced infrared (IR) imagers. Over the last few years major vendors, such as DRS, AIM, L-3, Cobham and Ricor developed and fielded new models for low cost (SWAP) cryocoolers in support of high operating temperature (150K and above) IR focal plane arrays.

It is worth noting that DRS [1,2], L3 [3] and Cobham [4] are following the traditional dual-piston (low vibration) compressor design concept, while Ricor [5-12] and AIM [13,14] favor a single-piston compressor offering lower SWAP and manufacturing expenses.

This decision has been substantiated by the choice of a relatively high driving frequency (100 Hz and above) leading to more compact design, smaller strokes and lower weight for the moving assemblies, resulting in lower the vibration export magnitudes. Along with these lines, the visual effect of high-frequency interference is less harmful. This favorable combination makes SWAP single-piston compressors adequate for the relatively heavy or fixedly mounted electro-optic payloads [15, 16].

In the case of inherently more vibration sensitive lightweight hand-held and gyro-stabilized payloads, the magnitudes of the cooler-induced vibration may be reduced by a payload design. In

Cryocoolers 19, edited by S.D. Miller and R.G. Ross, Jr.

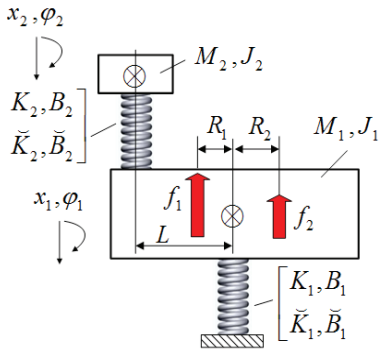

Figure 1. Dynamic model

gyro-stabilized applications, for example, the compressor and expander may be placed to minimize the moment about each gimbal axis.

When the design constraints prevent the prefered packaging or the payloads are sensitive to vibration, the cryocooler induced vibration may be efficiently attenuated to the acceptable levels using a Tuned Dynamic Absorber (TDA) mounted in-line with the compressor (major source of vibration export) to produce a counterbalancing force. This configuration will ultimately eliminate the translational dynamic response at the attachment point. Usually, it is advised to make such a TDA in the form of an undamped "mass-spring" single degree of freedom (SDOF) translational system, where the frequencies of tilting, in-plane translations, rotation about the axis are well separated from the frequency of the axial translational mode, which needs to be tuned exactly to the driving frequency (or vice versa), see [17,18]. Examples are known of cryogenically cooled long-range thermal weapon sights (TWS) or hand-held imagers, relying on the optional TDA [19,20].

Although the vibration export produced by the expander is relatively small, it cannot be disregarded in the light-weight hand held and gyrostabilized electro-optic applications. In these cases, the in-line mounting of the compressor and the expander units is favorable. Single-axis consolidation of the exported vibration induced by the compressor and the expander allows for effective use of a single, inline mounted translational TDA. Unfortunately, this option is not always practical due to the packaging constraints. For compactness, the expander and compressor are usually packaged side-by-side. In this case, the expander-induced exported vibration may produce a moment about the payload center of gravity resulting in an angular line-of-sight jitter and a translational defocusing.

The authors present a patent pending tunable Multimodal Tuned Dynamic Absorber (MTDA) with the translational frequencies and the two tilting mode frequencies are essentially tuned to the driving frequency. Dynamic analysis shows that the dynamic reactions (force and moment) produced by such a dynamic absorber are capable of simultaneously attenuatiing the translational and angular components of cryocooler induced vibration.

DYNAMIC MODEL, EQUATIONS OF MOTION AND ANALYSIS

Figure 1 shows the simplified four-degrees of freedom dynamic model, where the electro-optical payload having mass M_1 and moment of inertia J_1 is flexibly supported from the stationary base using a viscoelastic member featuring the linear and angular stiffness, and the damping $K_1, B_1; \breve{K}_1, \breve{B}_1,$ respectively.

It is further assumed that both the compressor and the expander are rigidly mounted to the payload frame at distances of R_1 and R_2 with respect to the center of gravity. The moving assemblies' reciprocating inside the compressor and expander have masses $m_{1,2}$. Their reciprocation with (fixed) angular driving frequency ω, magnitudes $\delta_{1,2}$ and constant phase lag φ result in a tonal force export, which may be thought of as a pair of coherent forces $f_1 = m_1\delta_1\omega^2 \sin(\omega t)$ and $f_2 = m_2\delta_2\omega^2 \sin(\omega t + \varphi),$ respectively.

The MTDA is schematically represented as a lumped body of mass M_2 and moment of inertia J_2, which is supported from the payload frame at a distance L with respect to the center of grav-

ity using viscoelastic member featuring linear and angular stiffness and damping $K_2, B_2; \breve{K}_2, \breve{B}_2$, respectively. The translation and tilt responses are x_1, φ_1 for the payload frame and x_2, φ_2 for the MTDA, respectively.

Differential equations of motion in time domain are as follows:

$$\begin{aligned}
&M_1\ddot{x}_1 + K_1x_1 + K_2\left(x_1 + L\varphi_1 - x_2\right) + B_1\dot{x}_1 + B_2\left(\dot{x}_1 + L\dot{\varphi}_1 - \dot{x}_2\right) = f_1 + f_2\\
&J_1\ddot{\varphi}_1 + \breve{K}_1\varphi_1 + K_2L\left(x_1 + L\varphi_1 - x_2\right) + \breve{K}_2\left(\varphi_1 - \varphi_2\right) + \breve{B}_1\dot{\varphi}_1 + B_2L\left(\dot{x}_1 + L\dot{\varphi}_1 - \dot{x}_2\right) + \breve{B}_2\left(\dot{\varphi}_1 - \dot{\varphi}_2\right) = f_1R_1 - f_2R_2\\
&M_2\ddot{x}_2 - K_2\left(x_1 + L\varphi_1 - x_2\right) - B_2\left(\dot{x}_1 + L\dot{\varphi}_1 - \dot{x}_2\right) = 0\\
&J_2\ddot{\varphi}_2 - \breve{K}_2\left(\varphi_1 - \varphi_2\right) - \breve{B}_2\left(\dot{\varphi}_1 - \dot{\varphi}_2\right) = 0
\end{aligned} \tag{1}$$

Complex Fourier transform, $G(j\omega) = \int_{-\infty}^{\infty} g(t)e^{-j\omega t}dt$, where $j = \sqrt{-1}$ is complex unity, yields a transition from time into a frequency domain $x_{1,2}(t) \Leftrightarrow X_{1,2}(j\omega)$, $\varphi_{1,2}(t) \Leftrightarrow \Phi_{1,2}(j\omega)$, $f_{1,2}(t) \Leftrightarrow F_{1,2}(j\omega)$. Substitution into (1) yields the set of 4 linear algebraic equations:

$$\begin{aligned}
&\left[-\omega^2M_1 + \left(K_1 + j\omega B_1\right) + \left(K_2 + j\omega B_2\right)\right]X_1 + \left(K_2 + j\omega B_2\right)\left(L\Phi_1 - X_2\right) = F_1 + F_2\\
&\left[-\omega^2J_1 + \left(\breve{K}_1 + j\omega\breve{B}_1\right) + \left(\breve{K}_2 + j\omega\breve{B}_2\right) + \left(K_2 + j\omega B_2\right)L^2\right]\Phi_1 + \left(K_2 + j\omega B_2\right)L\left(X_1 - X_2\right) -\\
&-\left(\breve{K}_2 + j\omega\breve{B}_2\right)\Phi_2 = F_1R_1 - F_2R_2\\
&\left[-\omega^2M_2 + \left(K_2 + j\omega B_2\right)\right]X_2 - \left(K_2 + j\omega B_2\right)\left(X_1 + L\Phi_1\right) = 0\\
&\left(-\omega^2J_2 + \breve{K}_2 + j\omega\breve{B}_2\right)\Phi_2 - \left(\breve{K}_2 + j\omega\breve{B}_2\right)\Phi_1 = 0
\end{aligned} \tag{2}$$

From the third and fourth equations of (2)

$$\Phi_1 = \frac{\left(-\omega^2J_2 + \breve{K}_2 + j\omega\breve{B}_2\right)}{\breve{K}_2 + j\omega\breve{B}_2}\Phi_2;\; X_1 = \frac{\left(-\omega^2M_2 + K_2 + j\omega B_2\right)}{K_2 + j\omega B_2}X_2 - \frac{\left(-\omega^2J_2 + \breve{K}_2 + j\omega\breve{B}_2\right)}{\breve{K}_2 + j\omega\breve{B}_2}L\Phi_2 \tag{3}$$

Substituting (3) into (1) eliminates X_1 and Φ_1 and yields a set of linear equations in X_2 and Φ_2

$$\begin{aligned}
&\mathbf{\Lambda}_{11}X_2 + \mathbf{\Lambda}_{12}L\Phi_2 = F_1 + F_2;\\
&\mathbf{\Lambda}_{21}X_2 + \mathbf{\Lambda}_{22}\Phi_2 = F_1R_1 + F_2R_2
\end{aligned} \tag{4}$$

where

$$\mathbf{\Lambda}_{11} = \frac{\left(-\omega^2M_2 + K_2 + j\omega B_2\right)\left[-\omega^2M_1 + K_1 + K_2 + j\omega B_1 + j\omega B_2\right] - \left(K_2 + j\omega B_2\right)^2}{K_2 + j\omega B_2};$$

$$\mathbf{\Lambda}_{12} = -\frac{\left(-\omega^2J_2 + \breve{K}_2 + j\omega\breve{B}_2\right)\left[-\omega^2M_1 + K_1 + j\omega B_1\right]}{\breve{K}_2 + j\omega\breve{B}_2}L;\; \mathbf{\Lambda}_{21} = -\omega^2M_2L;$$

$$\mathbf{\Lambda}_{22} = \frac{\left[-\omega^2J_1 + \breve{K}_1 + \breve{K}_1 + j\omega\breve{B}_2 + j\omega\breve{B}_1\right]\left(-\omega^2J_2 + \breve{K}_2 + j\omega\breve{B}_2\right) - \left(\breve{K}_2 + j\omega\breve{B}_2\right)^2}{\breve{K}_2 + j\omega\breve{B}_2}$$

Solution to (4) may be obtained by, say, using Kramer's rule

$$X_2 = \frac{\mathbf{\Delta}_{X_2}}{\mathbf{\Delta}};\Phi_2 = \frac{\mathbf{\Delta}_{\Phi_2}}{\mathbf{\Delta}} \tag{5}$$

where determinants are

$$\mathbf{\Delta} = \begin{vmatrix}\mathbf{\Lambda}_{11} & \mathbf{\Lambda}_{12}\\ \mathbf{\Lambda}_{21} & \mathbf{\Lambda}_{22}\end{vmatrix};\; \mathbf{\Delta}_{X_2} = \begin{vmatrix}F_1 + F_2 & \mathbf{\Lambda}_{12}\\ F_1R_1 + F_2R_2 & \mathbf{\Lambda}_{22}\end{vmatrix};\; \mathbf{\Delta}_{\Phi_2} = \begin{vmatrix}\mathbf{\Lambda}_{11} & F_1 + F\\ \mathbf{\Lambda}_{21} & F_1R_1 + F_2R_2\end{vmatrix}$$

Substituting (5) into (3) yields

$$\Phi_1 = \frac{\left(-\omega^2 J_2 + \breve{K}_2 + j\omega\breve{B}_2\right)}{\breve{K}_2 + j\omega\breve{B}_2}\frac{\mathbf{\Delta}_{\Phi_2}}{\mathbf{\Delta}};\; X_1 = \frac{\left(-\omega^2 M_2 + K_2 + j\omega B_2\right)}{K_2 + j\omega B_2}\frac{\mathbf{\Delta}_{X_2}}{\mathbf{\Delta}} - \frac{\left(-\omega^2 J_2 + \breve{K}_2 + j\omega\breve{B}_2\right)}{\breve{K}_2 + j\omega\breve{B}_2}L\frac{\mathbf{\Delta}_{\Phi_2}}{\mathbf{\Delta}} \quad (6)$$

Assuming the case of ideally tuned, MTDA $\left(K_2 = \omega^2 M_2;\; \breve{K}_2 = \omega^2 J_2;\; \breve{B}_2 \to 0;\; B_2 \to 0\right)$ from (5), we find finite values for translational and angular responses of MTDA at the driving frequency; these are:

$$X_2 \approx -\left(F_1 + F_2\right)/K_2;\; \Phi_2 \approx \left[-\left(F_1R_1 + F_2R_2\right) + L\left(F_1 + F_2\right)\right]/\breve{K}_2 \quad (7)$$

From (7), the force of dynamic reaction exerted by MTDA upon the payload frame is $\mathbf{Q} \approx K_2X_2 = -\left(F_1 + F_2\right)$, thus evidently counterbalancing aggregate force applied by the cryocooler. Along with these lines, the moment of dynamic reaction exerted by MTDA upon the payload frame is $\mathbf{T} \approx \Phi_2\breve{K}_2 = -\left(F_1R_1 - F_2R_2\right) + L\left(F_1 + F_2\right)$, thus evidently counterbalancing aggregate moment produced by the cryocooler along with the moment resulted from the MTDA translational motion.

Since X_2 and Φ_2 in (7) are finite, monotonous and almost constant functions in close vicinity to the driving frequency, we can use the below approximations

$$\Phi_1 \approx \frac{\left[-\left(F_1R_1 + F_2R_2\right) + L\left(F_1 + F_2\right)\right]}{\breve{K}_2^2}\left(-\omega^2 J_2 + \breve{K}_2 + j\omega\breve{B}_2\right); \quad (8)$$

$$X_1 \approx -\frac{\left(F_1 + F_2\right)}{K_2^2}\left(-\omega^2 M_2 + K_2 + j\omega B_2\right) - \frac{\left[-\left(F_1R_1 + F_2R_2\right) + L\left(F_1 + F_2\right)\right]L}{\breve{K}_2^2}\left(-\omega^2 J_2 + \breve{K}_2 + j\omega\breve{B}_2\right)$$

From (8), $\Phi_1 = 0$ and $X_1 = 0$ at the driving frequency, provided $K_2 = \omega^2 M_2$, $\breve{K}_2 = \omega^2 J_2$ and $\breve{B}_2 = B_2 = 0$. Also, from (8) the best geometrical location for the MTDA mounting is defined. Recalling that forces F_1 and F_2 are, generally speaking, complex numbers, we calculate the module of complex moment $\mathbf{T} = -\left(F_1R_1 - F_2R_2\right) + L\left(F_1 + F_2\right)$ and find the optimum value

$$L_{opt} = \frac{\left|F_1\right|^2 R_1 + \left|F_2\right|^2 R_2}{\left|F_2\right|^2 + 2\,\mathrm{Re}\left(F_2\right)\left|F_1\right| + \left|F_1\right|^2} \quad (9)$$

which minimizes its magnitude, where notation $\mathrm{Re}(*)$ means real part. It is worth noting that for the split Stirling linear cryocooler, the magnitude ratio F_2/F_1 is almost constant over the wide range of working conditions typical of the temperature control operational mode. From (9), the optimal position of MTDA will be, therefore, almost invariant over the range of working conditions.

For example, in the typical case $\varphi = 90\,\mathrm{deg}$ and $\mathrm{Re}\left(F_2\right) = 0$, thus

$$L_{opt} = \frac{\left|F_1\right|^2 R_1 + \left|F_2\right|^2 R_2}{\left|F_2\right|^2 + \left|F_1\right|^2};\quad \mathbf{T}_{\min} = \frac{\left|F_2\right|\left|F_1\right|}{\left|F_2\right|^2 + \left|F_1\right|^2}\sqrt{\left|F_1\right|^2\left(R_1 - R_2\right)^2 + \left|F_2\right|^2\left(R_1 + R_2\right)^2} \quad (10)$$

Figure 2 portrays the typical dependence of the moment $\mathbf{T}$ on the position of MTDA. The numerical values used in this example are: $\left|F_2\right| = 3N;\; \left|F_1\right| = 13N;\; \varphi = 90\,\mathrm{deg};\; R_1 = 35mm$ and $R_2 = -10mm$. From (10), when $L_{opt} = 32.7mm$ and $\mathbf{T}_{\min} = 0.13\,Nm$, this correlates well with the graph in Figure 2. This indicates the theoretical possibility of simultaneously attenuating the translation and tilting responses of the payload frame using a properly located, undamped single MTDA with matched translation and tilt frequencies.

In the most general case when $B_2 \neq 0;\; \breve{B}_2 \neq 0$, the entire analysis will be much more complicated. The numerical example below provides a practical insight into the attainable performance.

DYNAMIC DESIGN OF MUTIMODAL TDA

In this numerical example, the following set of variables will be used: $M_1 = 1\;kg;\; M_2 = 0.03\;kg;$ $J_1 = 0.0033\,kg\cdot m^2;\; J_2 = 0.000099\,kg\cdot m^2$. It is worth noting that such a MTDA adds only 3% to the total weight of the payload, the moment of inertia of such a MTDA is 3% of this payload. The payload is assumed to have a low frequency mount, thus mimicking the case of a hand-held infrared imager. Translational and tilting frequencies are assumed to be 10 Hz and damping ratios of 15%, respectively. The driving frequency is 105 Hz. The nominal frequencies of translational and tilting

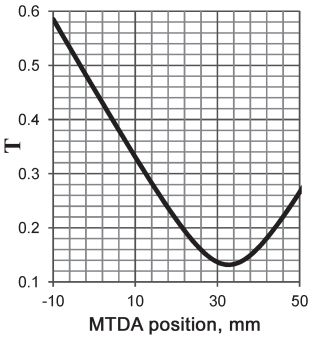

Figure 2. Optimal placement of MTDA

modes of MTDA will be equal to the driving frequency. The typical damping ratios for both modes will be conservatively assumed to be as low as 0.03%. The distances from the center of gravity are $R_1 = 0.035m$ and $R_2 = -0.01m$. Typical magnitudes for the force export are: $\|F_1\| = 13\ N$ and $\|F_2\| = 3N$, and the phase lag is assumed to be 90 deg.

In the reference case with no MTDA attached, the magnitudes of translation at the cold tip location and the tilt response of the payload are $27\mu m$ and $301\mu rad$, respectively. The magnitude of translation response is comparable to the typical focus depth and the magnitude of tilt response which is definitely higher than a typical acceptable value of $25\mu rad$. This substantiates the need for using a MTDA. Further, we consider the prior single degree of freedom (SDOF) TDA having only translational mode. The frequency of which is exactly tuned to the driving frequency. Translational and tilting response of the payload will be calculated at different TDA locations ranging from 10 mm to 50 mm relative to the payload center of gravity. Finally, we consider the two degrees of freedom (TDOF) MTDA featuring translational and tilting modes tuned exactly to the driving frequency. Translational and tilting responses of the payload will be calculated at different TDA locations ranging from 10 mm to 50 mm relative to the payload center of gravity.

Figures 3a and 3b compare the payload translation and tilt responses in the above three cases. In particular, the dashed lines represent the reference case with no TDA, double lines portray the case of thr SDOF TDA and the thick lines portray the case of TDOF TDA. From Figure 3, using SDOF TDA reduces both translation and tilt at the cold head location, the attenuation ratio is dependent on the TDA position with regard to the payload center of gravity. The optimal position is 33 mm, this is in accordance with Figure 2. It is clearly seen that SDOF TDA, even placed at the optimal position, is not capable of completely neutralizing the cooler-induced vibration. Such a TDA yields only a 4.6-fold and 9-fold attenuation of tilt and translation response at the location of cold head, respectively. Although the translational response is quite negligible in comparison with

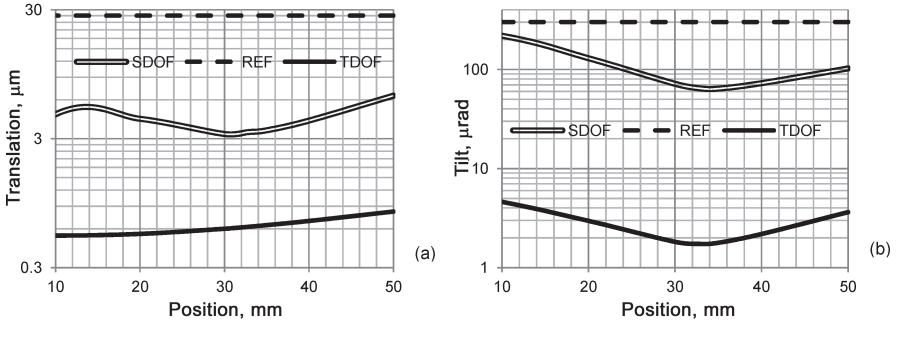

Figure 3. Translation and tilt responses of payload

the typical depth of focus, the achieved $65\ \mu rad$ magnitude of the payload tilt does not meet the requirement of $25\ \mu rad$ typical of a hand-held application.

The TDOF TDA is different from SDOF TDA. It yields an essential improvement: the attenuation ratios are much higher: 45-fold for translation and 176-fold for the tilt and the attained $1.7\ \mu rad$ tilt magnitude does meet the most stringent requirements. It is important to notice, that these improvements have been achieved without adding weight to the MTDA – just by making favorable use of its rotational inertia. It is also important to notice that the performance may be further improved by using an MTDA having a higher moment of inertia. Along these lines, optimal placement of TDA approximately corresponds to the location of compressor which allows placing the TDA in-line with compressor axis.

In the previous reasoning, we assumed that the resonant frequencies of translational and tilting modes were tuned exactly to the driving frequency, namely to 105 Hz. It goes without saying that in practice such accurate tuning will be very complicated. Therefore, prior to advising the mechanical design of MTDA we need to study the influence of frequency detuning on attainable performance. To start with, we will assume that the translational mode is tuned to the driving frequency 105 Hz exactly and vary the frequency of the tilting mode over the range 104.5-105.5 Hz.

Figure 4a shows the dependences of the magnitude of tilt and translation on the value of the tilting frequency at fixed translation frequency. The MTDA has been mounted inline with compressor at $L = 35mm$. From Figure 4a, tuning the tilting frequency results in essential attenuation of the tilt response, but this has very little influence on the translation response. Similarly, at the fixed and tuned tilting frequency, the tuning translation frequency results in essential attenuation of the translation response, but has very minor influence on the angular response (see Figure 4b). From Figure 4, the anti-resonant notches are wide enough to perform accurate frequency tuning and matching.

MECHANICAL DESIGN OF MUTIMODAL TDA

Figure 5 shows a diagrammatic view of the side-by-side split Stirling cryogenic cooler comprised of compressor 1 and expander 2 interconnected by the transfer line 3, whereupon the MTDA includes a primary proof ring 4 which is supported from one side by the flexural bearing 5 having central anchor for mounting to compressor housing 1. The secondary proof ring 6 is coaxial and displaceable along the primary proof ring; the outer diameter of the primary ring is tightly and slidably matched to the inner diameter of the secondary proof ring. In this preferable embodiment, the flexural bearing is made in the form of a circular planar spring with 4 symmetrical spiral slots.

In this embodiment, the translational frequency depends on the weight of the aggregate proof mass and axial spring rate of the flexural bearing. Along with these lines, the tilting frequencies depend on the angular spring rate of the said flexural bearing and moment of inertia of the aggregate proof mass. By finite elements design of the flexural bearing and proof rings, the said frequencies of the translation and tilting modes may be equalized and made essentially equal the fixed working frequency typical of the cryocooler.

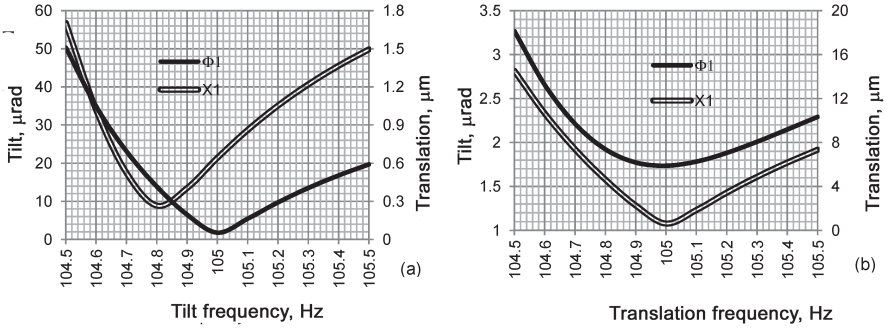

Figure 4. Translation and tilt response of payload at different frequency detuning.

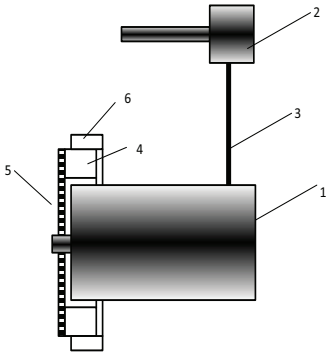

Figure 5. MTDA concept

Figure 6 shows the flexural bearing (a) and self-explanatory exploded view (b) of actual CAD design of such a TDA.

The modal analysis has been performed using the ANSYS 16.2 Finite Element software. Figure 7 shows the first 6 modal shapes: rotation about TDA axis (a), translation along the TDA axis (b), tilting modes (c,d) and in-plane modes (e,f). The frequencies of tilting and translation modes are 105 Hz. This has been achieved by virtually displacing the correction ring into particular position, it will be loosely set to "zero". The frequency of rotational mode is 65 Hz, the frequencies of the in-plane modes are 195 Hz.

Figure 8 shows the dependence of translation and tilt frequencies on the position of the secondary proof ring over the range from -0.5 mm to +0.5 mm relative to the above "zero" position. From Figure 8, the translation frequency (105 Hz) is not affected by the position of corrective proof ring while tilting frequencies vary simultaneously from 104.4 Hz to 105.5 Hz. It is also seen that at "zero" position all three frequencies are practically the same.

In practice, however, because of the manufacturing tolerances, on the spot fine frequency tuning is needed. This is achievable in two stages. First by precisely regulating the driving frequency and minimizing dynamic translation, the driving frequency is matched to the frequency of translation mode. Second by axially displacing the secondary proof ring relatively to the primary proof ring, this will alter the moment of inertia of the aggregate proof mass without altering its weight, and minimizing the angular dynamic response. The tilting frequencies may be accurately adjusted without affecting the translation frequency, to which the driving frequency has been accurately matched during the first stage.

Figure 9 shows the variation of angular and translational responses during the above explained tuning procedure performed with MTDA having initial translational and tilting frequencies 105 Hz and 105.4 Hz, respectively. Firstl by varying the driving frequency from 104.5 to 105.5 Hz, we find the minimum of the translation occurring at approximately 105 Hz. Figure 9a shows dependence

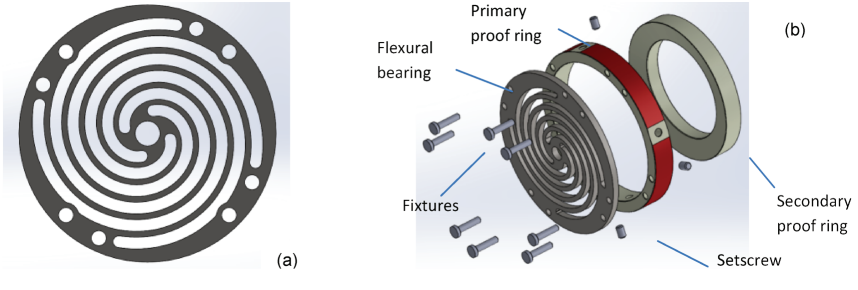

Figure 6. Design of MTDA

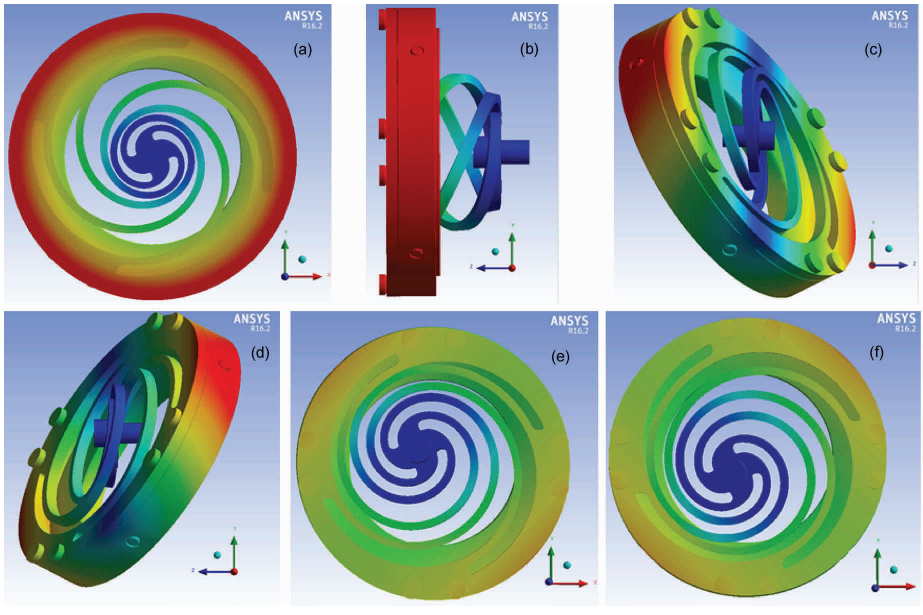

Figure 7. Dynamic modes

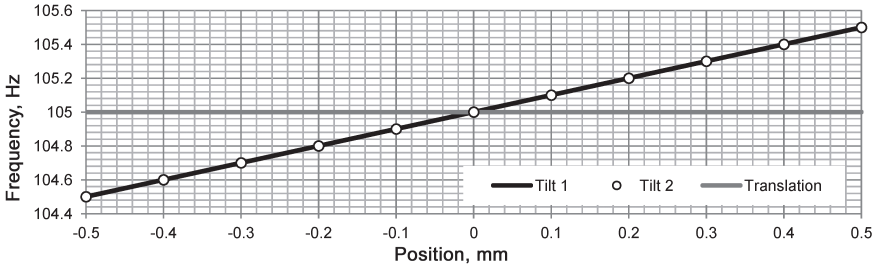

Figure 8. Resonant frequencies at different positions of corrective proof ring

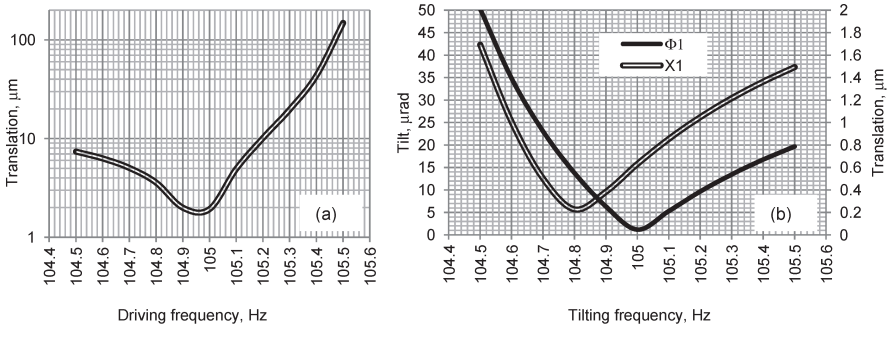

Figure 9. Scenario of tuning procedure

of payload displacement on the driving frequency with minimum of 1.93*mm* at 105Hz. Second at a fixed driving frequency of 105Hz, we axially displace the secondary proof ring and monitor the angular response using, say, an angular accelerometer. Figure 9b shows the appropriate dependence and optimum position of the secondary proof ring. From Figure 9b before tuning, the secondary

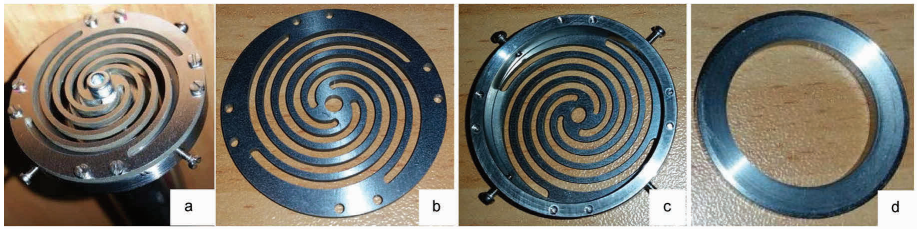

Figure 10. MTDA parts and assembly

proof ring is displaced from the optimum position by -0.5 mm; the linear response is 1.93 mm and angular response is 51 mrad. In the optimum position the angular response is 1.2 mrad and linear response is 0.6 mm. It is interesting to note that linear response is practically independent on the axial position of the correction proof ring.

FEASIBILITY STUDY: FINE MODAL TUNING

Figure 10 pictures the assembled (a) MTDA comprises of (b) flexural bearing, (c) primary proof ring with mounted flexural bearing and (d) secondary corrective proof ring.

Figure 11 shows the experimental setup for accelerance evaluation. The MTDA 1 is mounted upon the proof rod 2; the instrumented modal hammer 3 (Bruel&Kjaer Type 8206) is used for applying force (input) and accelerometer 4 (Endevko Type 752A12) is used for measuring resulting acceleration (output). The data acquisition and processing has been performed using dual-channel signal analyzer (Data Physics QUATTRO, not shown). As explained in [21], the location of typical antiresonance frequency in the module of accelerance of the combined system indicates the value of the resonant frequency of MTDA.

In Figure 12, the superimposed are spectra of moduli of translation and tilt accelerances. The typical anti-resonant notches corresponding to the translational and tilting frequencies of MTDA in both graphs are observed in the vicinity of the desired frequency 105 Hz. The secondary anti-resonant notch in the tilt accelerance corresponds to the in-plane mode at 193 Hz. By fine axially displacing the secondary proof ring precise matching the resonant frequencies is possible, as shown in Figure 13, where zoomed portions of the above accelerance are portrayed at different positions of the secondary proof ring, namely at -0.5 mm, 0 mm and +0.5 mm. It is worth noticing that the value of translational frequency is not affected by a position of the secondary ring.

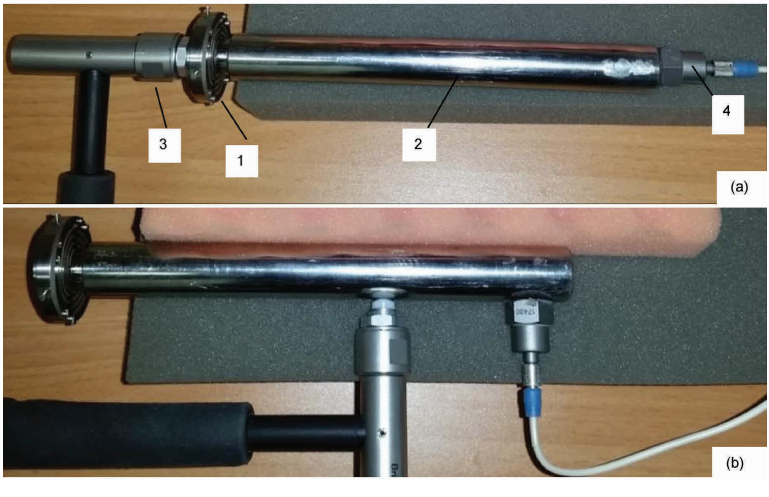

Figure 11. Evaluation of translation (a) and tilt (b) accelerances

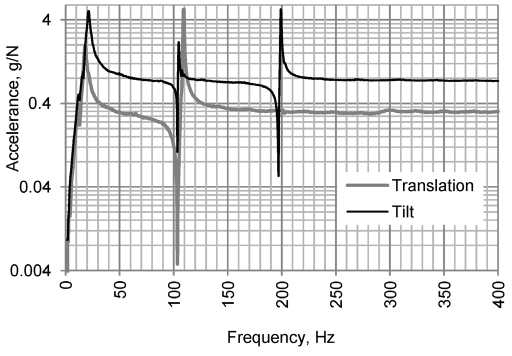

Figure 12. Tilt and translation accelerances

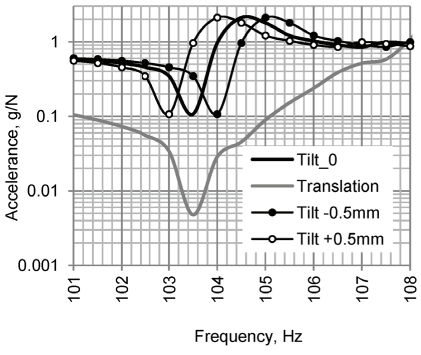

Figure 13. Fine frequency tuning

PRELIMINARY TESTING

Figure 14 shows the experimental setup. The miniature vibration exciter 1 is fixedly clamped on the top of vibration mounted platform 2 weighting approximately 2 kg. The MTTDA 3 is mounted collinearly but with essential (30mm) offset relatively to the exciter axis. The driving tonal signal is generated by the Data Physics QUATTRO signal analyzer 4 and amplified by the Ingenia Neptune digital servo drive (www.ingeniamc.com) 5. The Endevko Type 752A12 accelerometer 6 is mounted inline (b) and perpendicular to the shaker axis (c) and is used for measuring resulting dynamic response.

Figure 15 compares vibration spectra in axial (a) and perpendicular (b) directions with and with no MTDA . From Figure 15, in spite of the essential offset and small mass ratio, the impressive 70-fold vibration attenuation ratio has been achieved in both directions. In a tuned condition, the cooperative dual-mode operation of MTDA may be visually observed, as portrayed in Figure 16.

CONCLUSIONS AND FUTUTRE WORK

The analytical study has shown that MTDA has improved potential for essential attenuation of cryocooler induced line of sight jitter. The preliminary experimentation supported the approach to precise modal tuning. The authors are planning the full-scale experimental feasibility study.

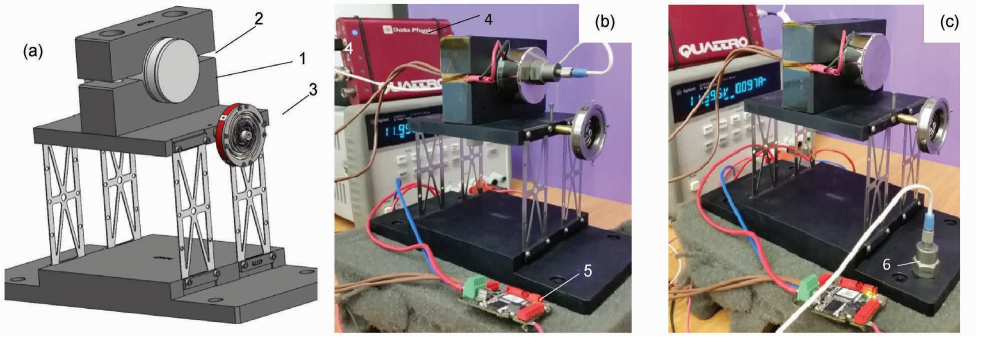

Figure 14. Experimental setup

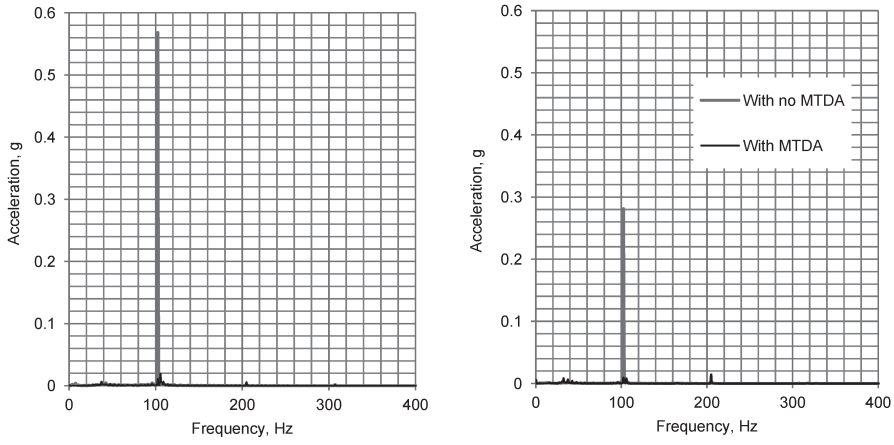

Figure 15. Experimental setup and attained performance

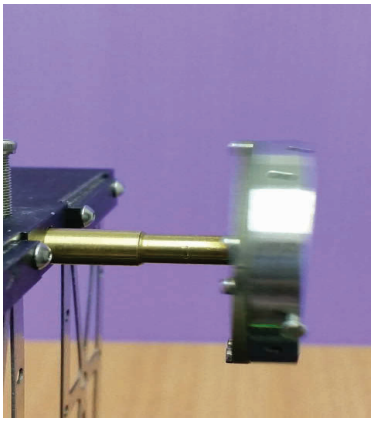

Figure 16. MTDA translation and tilt

REFERENCES

1. Rawlings, R. and Averitt, G., "A linear drive cryocooler for ultra-small infrared sensor systems," *Proc. SPIE* 9070, 90702R (2014).
2. http://www.drs.com/Products/RSTA/PDF/CD64012MWU.pdf
3. http://www.cinele.com/images/datasheets/ir_products/cryogenic_coolers3.pdf
4. http://www.cobham.com/about-cobham/mission-systems/about-us/life-support/davenport products/cryocooling-systems.aspx
5. http://www.ricor.com/products/split-linear/k527/
6. Veprik, A., Babitsky, V., Pundak, N. and Riabzev, S., "Vibration Control of Linear Split Stirling Cryogenic Cooler for Airborne Infrared Application", *Shock and Vibration*, 7 (6), 363-379 (2000)
7. Veprik, A., Vilenchik, H., Pundak, N., "Microminiature linear split Stirling cryogenic cooler for portable infrared imagers," *Cryocoolers 14*, ICC Press, Boulder, CO (2007), pp. 105-115.
8. Veprik, A., Vilenchik, H., Riabzev, S., Pundak, N., "Novel microminiature linear split Stirling cryogenic cooler for portable infrared imagers," *Proc. SPIE*, 6542, 65422F (2007)
9. Veprik, A., Zechtzer, S. and Pundak N., "Compact linear split Stirling cryogenic cooler for high temperature infrared imagers," *Cryocoolers 16*, ICC Press, Boulder, CO (2011), pp. 121-132.

10. Veprik, A., Zechtzer, S. and Pundak N., “Split Stirling linear cryogenic cooler for a new generation of high temperature infrared imagers,” *Proc. SPIE* 7660, 76602K (2010).

11. Veprik, A., Zechtzer, S., Pundak, N., Kirkconnell, C., Freeman, J. and Riabzev, S., “Adaptation of the low cost and low power tactical split Stirling cryogenic cooler for aerospace applications,” *Proc. SPIE* 8012, 80122J (2011).

12. Veprik A., Riabzev, S., Avishay, N., Oster, D., and Tuitto, A., “Linear cryogenic coolers for HOT infrared detectors,” *Proc. SPIE*. 8353, 83531V (2012)

13. Rühlich, I., Mai, M., Rosenhagen, C. et al., “Compact high-efficiency linear cryocooler in single-piston moving magnet design for HOT detectors,” *Proc. SPIE* 8353, 83531T (2012)

14. Rühlich, I., Mai, M., Withopf, A. et al., “AIM cryocooler developments for HOT detectors,” *Proc. SPIE* 9070, 90702P (2014)

15. Ashcroft, A.P., Richardson, L., Harji, J., and Giuliano, F., “Half-TV Format MWIR Sensor Module Incorporating Proximity Electronics,” *Proc. SPIE* 8353, 83530J-1 (2012)

16. http://www.finmeccanicausa.com/capabilities/Eclipse.aspx.

17. Ross, B. and Olan, R.W., “Passive balance system for machines”, USA Patent 5895033 A (1996)

18. Rosenhagen, C. and Rühlich, I., “Compensating oscillation device,” European Patent WO 2014206542 A1 (2014)

19. http://www.aim-ir.com/fileadmin/files/Data_Sheets_Thermal_sights/2013_neu/2013_AIM_ datenblatt_A4_HuntIR-K2_engl.pdf

20. http://elbitsystems.com/Elbitmain/files/LILY-L.pdf

21. Veprik, A., Tuitto, A., "Tuned dynamic absorber for split Stirling cryogenic cooler," *Proc. SPIE* 9821, Tri-Technology Device Refrigeration (TTDR), 98210F (2016)